PROCEEDINGS OF SPIE

SPIEDigitalLibrary.org/conference-proceedings-of-spie

Free strain gradient reversal of a variable recruitment fluidic artificial muscle bundle

Kim, Jeong Yong, Mazzoleni, Nicholas, Bryant, Matthew

Jeong Yong Kim, Nicholas Mazzoleni, Matthew Bryant, "Free strain gradient reversal of a variable recruitment fluidic artificial muscle bundle," Proc. SPIE 11586, Bioinspiration, Biomimetics, and Bioreplication XI, 115860L (22 March 2021); doi: 10.1117/12.2583213

SPIE.

Event: SPIE Smart Structures + Nondestructive Evaluation, 2021, Online Only

Free Strain Gradient Reversal of a Variable Recruitment Fluidic Artificial Muscle Bundle

Jeong Yong Kim, Nicholas Mazzoleni and Matthew Bryant
Department of Mechanical and Aerospace Engineering, North Carolina State University, Raleigh, NC USA 27695

ABSTRACT

This paper investigates the effect of *resistive forces* that arise in compressed fluidic artificial muscles (FAMs) within a variable recruitment bundle. Much like our skeletal muscle organs that selectively recruit different number of motor fibers depending on the load demand, a variable recruitment FAM bundle adaptively activates the minimum number of motor units (MUs) to increase its overall efficiency. A variable recruitment bundle may operate in different recruitment states (RSs) during which only a subset of the FAMs within a bundle are activated. In such cases, a difference in strain occurs between active FAMs and inactive/low-pressure FAMs. This strain difference results in the compression of inactive/low-pressure FAMs causing them to exert a resistive force opposing the force output of active FAMs. This paper presents experimental measurements for a FAM for both tensile and compressive regions. The data is used to simulate the overall force-strain space of a variable recruitment bundle for when resistive force effects are neglected and when they are included. Counterintuitively, an initial decrease in bundle free strain is observed when a transition to a higher RS is made due to the presence of resistive forces. We call this phenomenon the free strain gradient reversal of a variable recruitment bundle. The paper is concluded with a discussion of the implications of this phenomenon.

Keywords: Soft actuators, McKibben actuators, Fluidic artificial muscles, Variable recruitment, Resistive forces

1. INTRODUCTION

Soft actuators have become a topic of interest to many researchers due to its inherent compliance, high power density and flexibility in design. The McKibben actuator is a type of soft actuator that is often explored due to its simple yet unique working mechanism. It is commonly referred to as a fluidic artificial actuator (FAM), and it consists of an inner bladder and a double-helix braided mesh that is wrapped around it. As pressure is applied to the bladder, the kinematic constraint of the mesh allows the bladder to expand radially and contract axially. Although this mode of operation has been its original purpose when it was invented in the 1960s, researchers have developed twisting or bending actuators by adding inextensible layers to a McKibben actuator [1-2]. Others were able to reverse the direction of motion and create extensile actuators by changing the initial angle at which the braid is wrapped [3]. While these advancements were made by modifying the design of a McKibben actuator, others have explored the possibilities of using multiple FAMs in different configurations. Jenkins et al. investigated the advantages of orienting FAMs in a pennate configuration inspired from mammalian muscle topology [4]. Another bio-inspired configuration is the variable recruitment FAM bundle by Bryant et al. [5]. Multiple FAMs are oriented in parallel, similar to how our skeletal muscle organ consists of multiple units of actuation called muscle fibers. Each muscle fiber is activated by the firing of motor neurons. Depending on the desired load output of the muscle organ, a subset of muscle fibers is selectively recruited, for which the sequence of muscle fibers is determined by Henneman's Size Principle, which states that muscle fibers are recruited from smallest to largest in size [6]. A variable recruitment FAM bundle consists of multiple FAMs oriented in parallel that are grouped in motor units (MUs), which are the smallest units of actuation. Depending on which MUs are activated, the bundle operates at different recruitment states (RS). While conventionally, a single FAM is used as an independent actuator, a variable recruitment FAM bundle, as its nomenclature suggests, combines multiple FAMs in parallel to act as one actuator. This allows the bundle to tailor its active size to different load requirements. Typical FAM operation suffers from energy losses due to throttling down of pressure. A variable recruitment bundle has the capability to selectively recruit MUs and operate in the RS state that minimizes these losses, thus increasing the overall efficiency of the system [5]. Additionally, more precise control of force and strain is possible at lower RS due to decreased sensitivity to pressure changes [5].

Bioinspiration, Biomimetics, and Bioreplication XI, edited by Akhlesh Lakhtakia, Mato Knez, Raúl J. Martín-Palma,
Proc. of SPIE Vol. 11586, 115860L · © 2021 SPIE · CCC code: 0277-786X/21/$21 · doi: 10.1117/12.2583213

Recent studies have explored the effect of inactive and low-pressure MUs on the overall force output of the bundle [7, 8]. Prior analyses calculate the total bundle force output as the sum of forces generated by individual FAMs in the tensile region. However, by the nature of its operation, a variable recruitment bundle sometimes requires only a subset of its FAMs to be fully active while the rest are inactive or at low pressures. In such cases, the strain difference between active and inactive/low-pressure FAMs causes the latter to compress past its free strain condition, causing them to buckle. FAMs, in this compressive region, exert a *resistive force* that acts against the force output of active FAMs and need to be considered when calculating the overall force output of a bundle.

In this study, the resistive forces past free strain are measured for a FAM and compared to existing models in literature. The quasi-static force data from experiments are used to simulate the force-strain space of a variable recruitment FAM bundle with three recruitment states and compared to that of when resistive forces have been neglected. From this analysis, a phenomenon named *free strain gradient reversal* is observed.

1.1 Quasi-static modeling in the tensile region

Chou and Hannaford proposed a quasi-static force model based on the balance of virtual work done by force F and internal pressure P of the bladder which is expressed as:

$$-F\delta l = P\delta V \tag{1}$$

where δl is the variation of axial length and δV is the variation of the fluid volume inside the bladder. A kinematic relationship can be derived between the instantaneous radius r, and length l given as:

$$r = r_0\left(\frac{\sqrt{1-\cos^2\alpha_0\left(l/l_0\right)^2}}{\sin\alpha_0}\right) \tag{2}$$

where r_0 is the initial radius, l_0 is the initial length of the braided mesh, and α_0 is the initial braid angle of the mesh. By combining equations (1) and (2), the expression for F_{mesh} can be expressed in terms of the applied pressure P, and actuator strain ε.

$$F_{mesh} = \pi r_0^2 P\left(\frac{1}{\tan^2\alpha_0}\left(\varepsilon-1\right)^2 - \frac{1}{\sin^2\alpha_0}\right) \tag{3}$$

This force will be referred to in this paper as the mesh force, as it expresses the force due to the internal pressure that is converted into axial force using the kinematic constraints of the braided mesh. From this formulation, we can see that the force output is a function of strain. Although this model gives us the relationship between the pressure and the axial force output of the actuator due to the kinematic constraint imposed by the braided mesh, it is not able to predict the pressure-dependent nature of free strain. For a given pressure, maximum actuator force occurs at zero strain, which is also known as the blocked force condition. The strain at which the force is zero is known as the free strain, which is constant for all pressures when using (3). This pressure-dependent nature of free strain can be accounted for by the bladder elastic forces that oppose the mesh force output. Therefore, the bladder elastic forces are an integral component in understanding the force-strain relationship. Klute and Hannaford use the Mooney-Rivlin strain energy function W, and apply the principle of virtual work to model the elastic bladder force [9]. Including the elastic bladder force term, the total force of a FAM is expressed as:

$$F_{total} = F_{mesh} + F_{bladder} = P\frac{dV}{dL} - V_b\frac{dW}{dL} \tag{4}$$

1.2 Resistive force in the compressive region

The development of these models does not consider the effect of resistive forces, as typically the forces exerted by the FAM to its surroundings is not of concern. Both ideal and Klute-Hannaford models can be extended past the free strain to

yield negative forces. However, these forces are not representative of the actual resistive forces because FAMs undergoing compression experience phenomena such as buckling and collapse of the bladder. Kim et al. presents a qualitative observation of the bladder behavior past free strain and divides resistive forces into distinct regions [7]. Based on observation, a FAM under compression is divided into a post-buckling region that starts as the FAM is in compression until the next region, which is the post-collapse region. In this region, the bladder has undergone significant bending so that the hollow cylindrical bladder has collapsed into a hinge. It was reported that the collapse results in a significant decrease in the magnitude of resistive force, which current models are not able to predict. The study poses a need for the modeling of resistive forces that will not be discussed in the scope of this study. For the purposes of this study, which is to explore the effects of resistive forces on a variable recruitment bundle, experimentally obtained values will be used to simulate the bundle force-strain space.

2. EXPERIMENT RESULTS AND DISCUSSION

2.1 Experiment setup

The quasi-static force and strain of a FAM was measured. The FAM had an initial radius of 0.0635 m (1/2 in.), initial braid angle of 33 degrees, and a bladder thickness of 0.00159 m (1/16 in.). The FAM had an initial length of 0.127 m (5 in.) corresponding to a slenderness ratio of 10. The experiments were conducted on a linear dynamometer designed and built by Chipka et al. as shown in Figure 1 [10]. It consists of a hydraulic drive cylinder that is controlled using a servo value (MOOG Series G761-3005B) and position feedback from a linear variable differential transformer (LVDT). The force generated by the FAM was measured by a load cell (Transducer Techniques SSM-1K). The pneumatic pressure supplied to the FAM was measured using pressure transducers and controlled using servo valves (FESTO MPYE-5-M5-010-B). The FAM was pressurized from 0 kPa to 413.7 kPa (60 psi) in 68.1 kPa (10 psi) intervals. The maximum free strain of the bundle was measured by applying the maximum testing pressure and used as a reference for which all FAMs were compressed to. The FAM was constrained by the end plates at its initial length then the desired pressure was applied. The position of the drive cylinder was controlled in a sufficiently slow rate as to eliminate any dynamic effects. The force was measured from the blocked force condition and past the free strain condition until the maximum bundle free strain.

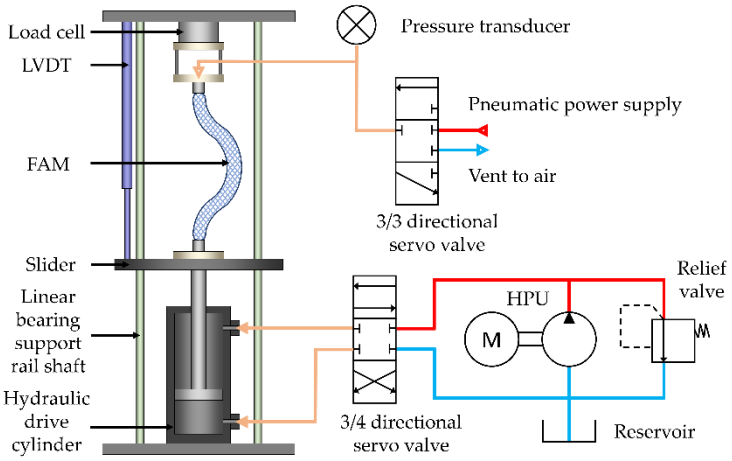

Figure 1. Experiment setup using the LHD developed by Chipka et al. [**10**]. A hydraulic power supply is used to actuate the drive cylinder. The FAM is activated using a pneumatic power supply while the force and contraction is measured using a load cell and LVDT, respectively.

2.2 Experimental results for resistive force and comparison to existing models

Figure 2(a) shows the results for all the measured pressures from 0 kPa to 413.7 kPa. While typically, only the forces generated by the FAM (i.e. positive forces) would be of interest, the FAM in this experiment was compressed past its free strain into the negative force region. To better illustrate the resistive forces, the force curves for 0 kPa and 68.1 kPa are shown in comparison to the ideal and Klute-Hannaford models in Figure 1(b). The experimental results show a decrease in resistive force magnitude due to buckling, then collapse of the bladder. This happens around 0.05 strain for the 0 kPa case and 0.2 strain for the 68,1 kPa case. For 68.1 kPa, the ideal model over predicts both the blocked force and free strain.

For 0 kPa, the ideal force model does not consider any elastic forces of the bladder and therefore remains zero. The Klute-Hannaford model similarly over predicts the blocked force and free strain but shows a smaller discrepancy in free strain compared to the ideal model. Additionally, the Klute-Hannaford model is able to predict a negative force for 0 kPa. However, the magnitude of resistive forces predicted by the Klute-Hannaford model is predicted to be greater than the measured values. More importantly, the ideal or Klute-Hannaford models are not able to predict the decrease in resistive force magnitude due to buckling. As a result, the discrepancy between model and experiment is accentuated at higher strains.

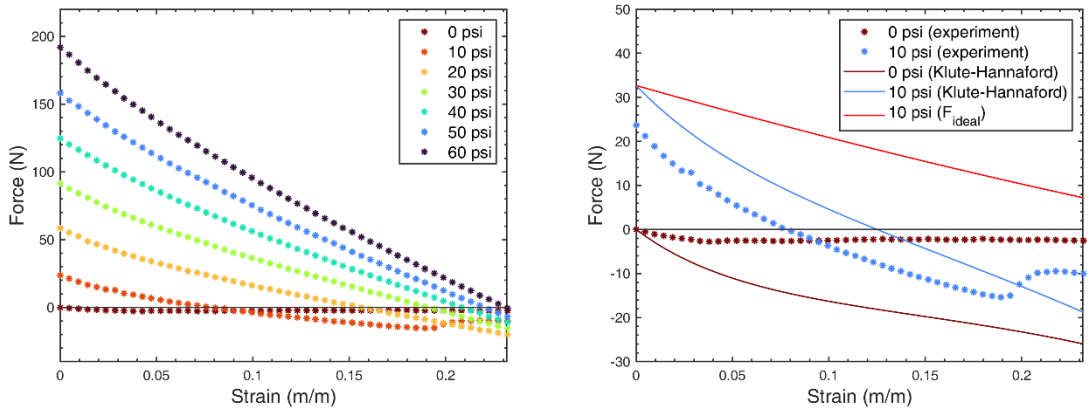

Figure 2. Experimental results of quasi-static force measurement for applied pressures of 0 kPa to 413.7 kPa. (a) Both the tensile forces generated by the FAM (positive) and the resistive forces (negative) are shown. (b) A closer view of the force curves for 0 kPa and 68.1 kPa are shown along with results from the ideal model and the Klute-Hannaford model.

2.3 Effect of resistive force on overall performance of a variable recruitment bundle

Figure 3 shows the isobaric force-strain curves for a variable recruitment bundle with two recruitment states (RS) for two cases: when experimental data is used but resistive forces are neglected and when experimental data is used including resistive forces. The isobaric force curves in the first and second recruitment states are plotted in green and blue, respectively. Once the first RS is fully activated, the bundle enters the second RS, during which the first MU stays at its maximum pressure and the second MU is either partially or fully activated. Figure 3(a) shows the force-strain space for a bundle neglecting resistive forces. The force-strain spaces for RS 1 and RS 2 are distinctly divided by the isobaric force curve for the maximum pressure of RS 1. The most notable difference between the two cases is observed in the overlapping region between RS 1 and RS 2 in Figure 3(b). The overlapping region is more prominent for strains near maximum bundle free strain. Figures 3 (c) and (d) show a closer view of this area with the applied pressures for MU 2 indicated for each isobaric curve. In the case when resistive forces are neglected, any increase in MU 2 pressure increases the force for the same value of strain. Thus, for a specific force–strain output, the required operating state of the bundle can be easily categorized into either RS 1 or 2. However, when resistive forces are included in the overall bundle force, an increase in the pressure of MU 2 does not necessarily result in an increase in force. As the transition is made from RS 1 to 2, the pressure of MU 2 is zero, which overlaps with the force curve of MU 1 at maximum pressure. However, an increase of MU 2 pressure to kPa actually decreases the force near strains of 0.195. Both the force generated and the free strain of the overall bundle decrease. The decrease in force can be accounted for by the negative resistive forces of the FAMs that are in compression due to the difference in strain between the fully active MU 1 and the low-pressure MU 2. The free strain decreases until the pressure of MU 2 increases until a certain value and begins to increase as the difference in strain between MU 1 and 2 becomes smaller. The effect of this phenomenon is discussed in further detail in Section 2.4.

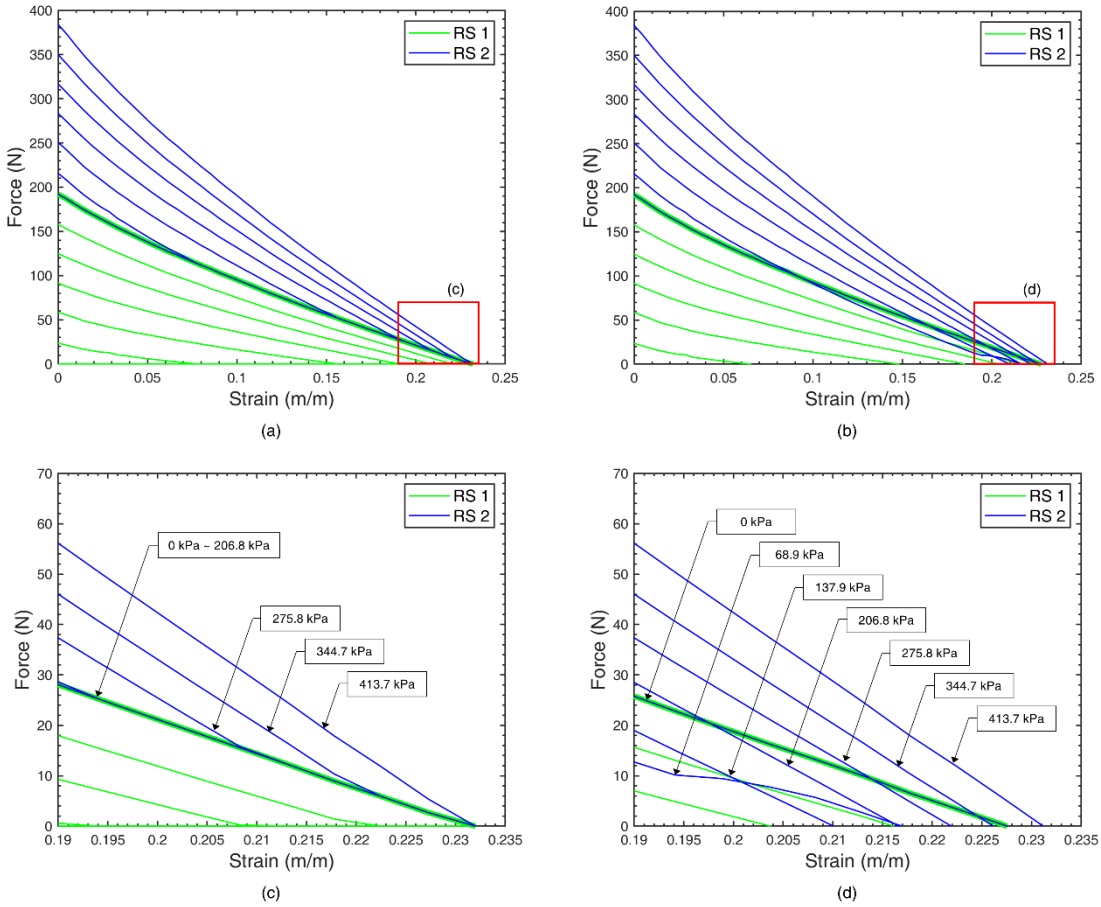

Figure 3. Force-strain space of a variable recruitment bundle with two motor units (MUs) when (a) resistive forces neglected, and (b) resistive forces included. (c) and (d) show zoomed-in views of the force-strain space near maximum strain with resistive forces neglected and included, respectively.

2.4 Free strain gradient reversal of a variable recruitment bundle

The key difference between the force-strain plots of a variable recruitment bundle when resistive forces are neglected and when they are included is clearly illustrated by plotting the free strain of the bundle with respect to the change in pressure of MU 2. After the first MU is fully activated (i.e. reaches maximum pressure), the bundle transitions from its first RS to the second. In the second RS, the pressure of MU 2 increases starting from zero to the maximum source pressure. When resistive forces have been neglected, the bundle free strain simply remains constant, as shown in Figure 4. There is a difference in free strain predicted by the ideal model and the Klute-Hannaford model due to the consideration of elastic forces. However, experimental results show that free strain is not constant; instead, free strain initially decreases as MU 2 pressure increases, before eventually increasing back to the original free strain of a single MU when MU 2 pressure is zero. We call this phenomenon the *free strain gradient reversal* of a variable recruitment bundle. This is of particular interest with regard to the control of bundle force and strain. Jenkins et al. developed an online variable recruitment controller and investigated its effectiveness for orderly and batch recruitment schemes for a variable recruitment bundle when resistive forces were not considered [11]. As discussed in Section 2.3, there exists an overlapping region between RS 1 and 2 that poses a new challenge in terms of designing a RS switching algorithm. In terms of bundle design, Mazzoleni et al. investigated the use of tendons to mitigate the effects of resistive forces compared to the conventional fixed-end configuration [8]. Although the tendon configuration was able to mitigate the adverse effects of resistive force, the packaging constraint imposed on the two configurations resulted made the initial FAM length shorter with the presence of tendons and resulted in a lower overall bundle free strain.

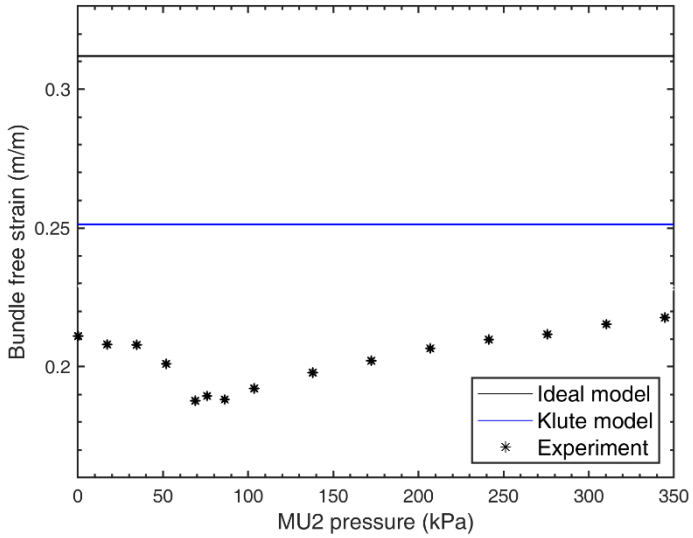

Figure 4. Free strain of actuator bundle versus pressure applied to motor unit (MU) 2 shown for the ideal model, the Klute-Hannaford model [9], and experimental data. The pressure of MU 1 is kept constant at 344.7 kPa. The free strain initially decreases in response to increased pressure in the second recruitment state.

3. CONCLUSION

This study presents experimental measurement of force for a McKibben actuator in the tensile and compression regions. While the isobaric force curves in the tensile region show the typical pressure-dependent blocked force and free strain behavior established by other models in the literature, forces in the compression region show how the FAM exerts a resistive force as it is being deformed into a buckled shape. The effect of resistive forces is explored in the context of a variable recruitment bundle to show how these forces affect bundle free strain. While the increase in applied pressure is typically associated with an increase in force, the presence of resistive forces decreases the overall force output of a bundle immediately after a transition to a higher RS is made. This is due to the pressure-dependent free strain behavior of FAMs that cause a difference in strain between active and inactive/low-pressure MUs.

REFERENCES

[1] Tondu, B. Modeling of the McKibben artificial muscle: A review. J. Intell. Mater. Syst. Struct. **2012,** 23, 225-253. 10.1177/1045389x11435435

[2] Al-Fahaam, H.; Davis, S.; Nefti-Meziani, S. The design and mathematical modeling of novel extensor bending pneumatic artificial muscles (EBPAMs) for soft exoskeletons. **2018,** 99, 10.1016/j.robot.2017.10.010

[3] Ohta, P.; Valle, L.; King, J., et al. Design of a Lightweight Soft Robotic Arm Using Pneumatic Artificial Muscles and Inflatable Sleeves. **2018,** 5, 204-215. 10.1089/soro.2017.0044

[4] Jenkins, T., Bryant, M. Pennate actuators: force, contraction and stiffness. Bioinspir. Biomim. **2020**, 15, 046005. 10.1088/1748-3190/ab860f

[5] Bryant, M.; Meller, M. A.; Garcia, E. Variable Recruitment Fluidic Artificial Muscles: Modeling and Experiments. **2014,** 23, 74009. 10.1088/0964-1726/23/7/074009

[6] Henneman, E.; Somjen, G.; Carpenter, D. O. Excitability and inhibitability of motoneurons of different sizes. J Neurophysiol. **1965**, 28, 599-620. 10.1152/jn.1965.28.3.599.

[7] Kim, J. Y.; Mazzoleni, N.; Bryant, M. Investigation of Resistive Forces in Variable Recruitment Fluidic Artificial Muscle Bundles. Conf. Proc. Soc. Exp. Mech. **2021**, 8, 305-313. 10.1007/978-3-030-47717-2_32.

[8] Mazzoleni, N.; Jeong, Y. K. and Bryant, M. The effect of resistive forces in variable recruitment fluidic artificial muscle bundles: a configuration study. Proc. SPIE, Bioinspiration, Biomimetics, and Bioreplication X **2020,** 11374. 10.1117/12.2557907

[9] Klute, G.; Hannaford, B. Accounting for Elastic Energy Storage in McKibben Artificial Muscle Actuators. ASME. J. Dyn. Syst. Meas. Control. **2000**, 122, 386-388. 10.1115/1.482478.

[10] Chipka, J.; Meller, M. A.; Volkov, A.; Bryant, M.; Garcia, E. Linear dynamometer testing of hydraulic artificial muscle with variable recruitment. J. Intell. Mater. Syst. Struct. **2017,** 28, 2051-2063. 10.1177/1045389X16682845

[11] Jenkins, T. E.; Chapman, E. M.; Bryant, M. Bio-inspired online variable recruitment control of fluidic artificial muscles. Smart Mater. Struct. **2016**, 25, 125016. 10.1088/0964-1726/25/12/125016.